PERGAMON

International Journal of Heat and Mass Transfer 45 (2002) 1631–1642

International Journal of HEAT and MASS TRANSFER

www.elsevier.com/locate/ijhmt

Unsteady forced convection with sinusoidal duct wall generation: the conjugate heat transfer problem

James Sucec *

Department of Mechanical Engineering, University of Maine, 5711 Boardman Hall, Room 202, Orono, ME 04469-5711, USA

Received 28 November 2000; received in revised form 23 August 2001

Abstract

Transient heat transfer solutions are found for a fluid flowing within a parallel plate duct when there is sinusoidal generation with axial position in the duct wall. Solutions are found for wall temperature, surface heat flux and fluid bulk mean temperature as a function of position and time in this conjugated problem. To develop this solution, finite difference methods are used as well as the quasi-steady method and another method which employs a two integral representation for the surface heat flux. Accuracy limitations of the quasi-steady results are identified. Transient local Nusselt number predictions show its dependence upon time.

1. Introduction

Unsteady state heat transfer conditions occur in duct fluid and walls of equipment such as nuclear fuel element cooling passages, electric resistive heaters and heat exchangers. Startup and shutdown operations, as well as changes in steady-state power levels, give rise to the transient conditions in the duct wall and flowing fluid.

Most of these situations are conjugated problems, that is, one cannot prescribe either the surface temperature or surface heat flux variation with time and position. Hence these quantities, along with the bulk mean temperature distribution within the fluid, all must be predicted using the "conjugation conditions", namely, that the temperature and heat flux must be continuous at the common boundary of the fluid and the wall.

Previous solutions to unsteady, conjugate laminar flow duct problems include the finite difference solutions of Schutte et al. [1], Al-Nimr and Hader [2], Yan et al. [3] and Lin and Kuo [4], as well as the eigenfunction solution of Olek [5]. In all of these, the boundary condition at the outer surface was either a step change in temperature or in heat flux. Finite difference solutions involving convection at the outer boundary were developed by Yan [6] and Sucec [7]. Travelho and Santos [8], used Laplace transforms to solve slug flow in the duct and Guedes et al. [9] applied generalized integral transforms to turbulent duct flow. Both [8] and [9] are for a periodic inlet temperature variation with time. In a very early work, Siegel [10], used a slug flow velocity profile and numerical integration along characteristic curves to solve some cases involving wall generation. A recent example of the quasi-steady approach is the work of Romie [11]. Accuracy of quasi-steady predictions is often limited by the wall–fluid thermal capacity ratio and the "speed" of the transient.

In the present work, space and time dependent generation rates per unit volume, q''', within the wall material are considered. For the most part, we will deal with, primarily, the first time domain, that is, where time $t < x/u_{\max}$. This is the time it takes the fastest moving fluid to travel from the duct entrance to the position, x, of interest. This time period is the initial stage of the transient and is often the time when the most rapid changes with time occur. The primary solution method will be the finite difference solution of the partial differential energy equations for the flowing fluid and the duct wall material. This baseline finite difference solution will be compared to results which use the quasi-steady method, and, also, to a two integral, approximate surface heat flux expression, developed in [12]. The generation rates, within the wall material, used in the

* Tel.: +1-207-581-2124; fax: +1-207-581-2379.
E-mail address: rme700@maine.edu (J. Sucec).

0017-9310/02/$ - see front matter
PII: S0017-9310(01)00275-7

Nomenclature

a_0, a_1	coefficients in velocity profile, Eq. (22)
A_2	coefficient given in Appendix A
b	duct wall thickness
$b_0, b_1, b_2,$	
b_3, b_6	coefficients given in Appendix A
B	$\rho_w c_{pw} b/\rho_f c_{pf} R$, ratio of thermal capacity of the wall to the fluid
c_{pf}, c_{pw}	specific heat capacity of fluid and of wall
C_R	coefficient in generation expression, Eq. (6)
$C_S, C_C,$	coefficients given in Appendix A
D	defined by Eq. (7)
f	q'''/q_g
F	$\alpha_f t/R^2$ nondimensional time
F_a, F_b	defined in Eq. (28)
g_S, g_{CA}, g_{CB}	coefficients defined by Eqs. (18)–(20)
G_C, G_S	coefficients given in Appendix A
h	surface coefficient of heat transfer at inside duct wall
i	index
j	index
J	defined in Eq. (17)
k	index
k_f, k_w	thermal conductivity of fluid and wall, respectively
K	defined by Eqs. (6) and (7)
M	defined by Eq. (30)
n	index
Nu	hR/k_f, Nusselt number
p	Laplace transform parameter
q_w	heat flux at inside wall
q_g	reference generation rate per unit volume (W/ m^3)
q'''	energy generation rate per unit volume (W/m^3)
Q	$q_w/q_g b$ nondimensional inside surface heat flux
R	half height of duct
R_k	defined in Eq. (28)
R_n	R_k at $k = n$
S_k	defined in Eq. (29); $S_n = S_k$ at $k = n$
t	time
T, T_i, T_B, T_W	local, initial, bulk mean and wall temperatures
u_m, u_{max}	mass average and maximum velocity
W	defined in Eq. (13)
x	space coordinate along the wall
X	$\alpha_f x/R^2 u_m$ nondimensional x coordinate
y	space coordinate perpendicular to duct wall
Y	y/R nondimensional y coordinate

Greek symbols

α_f	thermal diffusivity of fluid
Δf	$\alpha_f \Delta t/R^2$
$\Delta f, \Delta X$	finite difference increments in F and X
ρ_f, ρ_w	mass density of fluid and of wall
σ	dummy variable for F
τ	$F - X$
ϕ	$k_f(T - T_i)/q_g bR$ nondimensional local temperature
ϕ_B, ϕ_W	bulk mean fluid and wall value of ϕ

Subscripts

B	bulk mean fluid value
qs	quasi-steady value
w	duct wall value

present work are both sinusoidal in the axial coordinate, x, with one of them also being an exponential function of time, t. The sinusoidal variation in x is an important one in nuclear fuel plates, [10]. [13], argues for a sinusoidal variation with x to model a periodic array of heating elements within a wall. In an earlier work, Sucec and Weng [14], use a simpler generation rate, q''', which allowed an analytical solution when using the approximate flux model.

2. Analysis

The physical situation is a parallel plate duct of wall thickness b and distance R to the duct midplane. A constant property fluid flows within the duct with a steady fully developed, laminar velocity profile. The Peclet number is high enough so that axial conduction is negligible as is viscous dissipation. The temperature profile is, in general, undeveloped and the Biot number is low enough to neglect transverse temperature gradients within the wall. At time $t = 0$, the fluid and the wall material are at the constant temperature T_i, when, suddenly, the internal generation rate within the wall, q''', becomes active and is a function of both axial coordinate, x, and time, t, in general. We want the solution to yield the local wall temperature, surface heat flux and fluid bulk mean temperature as a function of axial position and time t. These will allow the calculation of the local Nusselt number if it is desired. Both the approximate solution which uses the two integral flux model and the quasi-steady solution are, strictly speaking, valid only in the first time domain, $t < x/u_{max}$. The finite difference solution has no

such limitation and also is not limited to the thermal entrance region.

The generation rate, q''', is rewritten as $q''' = q_g f(x,t)$ where both q''' and q_g have the same units, W/m^3. Using this in an energy balance on the duct wall, b by dx, gives the following differential equation where $q_w(x,t)$ is the local surface heat flux, W/m^2:

$$\rho_w c_{pw} b \frac{\partial T_w}{\partial t} + q_w(x,t) = q_g f(x,t). \tag{1}$$

Eq. (1) is the basic wall energy balance to be used in all three of our approaches to a solution. Used throughout the paper are non-dimensional quantities defined by $F = \alpha_f t/R^2$, $Y = y/R$, $X = \alpha_f x/R^2 u_m$, $Q = q_w/q_g b$, $\phi_w = k_f(T_w - T_i)/q_g bR$, $\phi_B = k_f(T_B - T_i)/q_g bR$ and $B = \rho_w c_{pw} b/\rho_f c_{pf} R$.

2.1. Finite difference analysis

An energy balance on the flowing fluid gives the following partial differential equation for the fluid temperature, $\phi(X,F)$:

$$\frac{\partial \phi}{\partial F} + 3\left[Y - .5Y^2\right]\frac{\partial \phi}{\partial X} = \frac{\partial^2 \phi}{\partial Y^2}. \tag{2}$$

The initial condition and boundary conditions are as follows:

$$\begin{aligned} &F = 0, \quad X > 0, \quad 0 \leqslant Y \leqslant 1, \quad \phi = 0,\\ &X = 0, \quad F > 0, \quad 0 < Y \leqslant 1, \quad \phi = 0,\\ &Y = 1, \quad F > 0, \quad X > 0, \qquad \partial\phi/\partial Y = 0. \end{aligned} \tag{3}$$

Closure of the mathematical problem statement is achieved by using the wall energy balance, Eq. (1), and combining it with the two conjugation conditions at $Y = 0$, namely equal surface temperatures and equal heat fluxes in both the fluid and the solid wall, which yields the following condition:

$$\begin{aligned} &Y = 0, \quad X > 0,\\ &\qquad F > 0 - \left(\frac{\partial \phi}{\partial Y}\right) + B\frac{\partial \phi}{\partial F} = \frac{q'''}{q_g} = f(X,F). \end{aligned} \tag{4}$$

Using $X = i\Delta X$, $Y = (j-1)\Delta Y$ and $F = n\Delta f$, the following implicit finite difference equation is used to simulate Eq. (4), at $Y = 0$, or $j = 1$:

$$\left(1 + \frac{\Delta f}{B\Delta Y}\right)\phi_{i,1}^{n+1} - \frac{\Delta f}{B\Delta Y}\phi_{i,2}^{n+1} = \phi_{i,1}^{n} + \frac{\Delta f}{B} f(X,F). \tag{5}$$

The finite difference equations for the interior fluid nodes, $j = 2$ to N, are given in [7] as Eqs. (8) and (9). Discussion of the study of compatibility, truncation error and stability of these implicit finite difference equations is available in [7]. In the present work, lattice refinement studies led to the lattice spacings, $\Delta X, \Delta Y, \Delta f$, needed to insure that the solution is sensibly independent of these lattice spacings. These spacing sizes, in general, depend upon the case being considered and on the values of dimensionless time, F, and axial position, X. For a typical set of conditions, for example, when $q''' = q_g[e^{DF} - 1]\sin \pi KX$, $D = 4.0$, $K = 1.0$ and $B = 1.0$, lattice refinement led to the choice of 193 nodes across the duct half width in the Y direction, $\Delta X = .003125$ and $\Delta f = .00015625$. Using these spacings, the maximum change in ϕ_w, ϕ_B, and Q is less than 0.22% if the lattice is refined further.

2.2. Generation rate forms

The finite difference equations described above were solved using the following two functions for the dimensionless generation rate, $f(X,F)$, where $q'''/q_g = f(X,F)$. The first of these is independent of time, F, and therefore is a model for a steady-state generation function, while the second has exponential dependence upon time F in addition to its X dependency.

$$f(X) = (1 + C_R \sin \pi KX), \tag{6}$$

$$f(X,F) = (e^{DF} - 1)\sin \pi KX. \tag{7}$$

Eq. (7) can be used to model either an initial startup or a change in the steady-state power level. For example, Eq. (7) may model $f(X,F)$ when the initial state is $F = 0$ and Eq. (7) is used until F reaches F_e, the value that gives the ultimate desired steady-state power level.

2.3. Quasi-steady analysis

This approach, which is approximate, is usually the easiest method for solving unsteady state convection problems. Here, in the wall energy balance, Eq. (1), the surface heat flux is represented with Newton's cooling law using the constant, steady state, fully developed value of the surface coefficient, h. This gives the following differential equation for the wall temperature, where the Nusselt number used is $Nu = hR/k_f$.

$$B\frac{\partial \phi_W}{\partial F} + Nu(\phi_W - \phi_B) = f(X,F). \tag{8}$$

The energy balance on the flowing fluid yields the differential equation for the fluid bulk mean temperature in this quasi-steady analysis and this is followed by the initial and boundary conditions for Eqs. (8) and (9):

$$\frac{\partial \phi_B}{\partial F} + \frac{\partial \phi_B}{\partial X} = Nu(\phi_W - \phi_B), \tag{9}$$

$$\begin{aligned} &F = 0, \quad X > 0, \quad \phi_B = \phi_W = 0,\\ &X = 0, \quad F > 0, \quad \phi_B = 0. \end{aligned} \tag{10}$$

2.4. Quasi-steady solution

Eqs. (8)–(10) were solved first using the generation given in Eq. (6). This was done by taking the Laplace transform of these equations with respect to F and eliminating $\bar{\phi}_w$ between Eqs. (8) and (9) where $\bar{\phi}_w$ is the transform of $\phi_w(X,F)$.

This gave an ordinary differential equation for $\bar{\phi}_B(X,p)$ which was solved. Then, since we are interested in a first time domain solution, that is, relatively small times F, therefore large values of the transform parameter p, some simplifications were possible and finally led to the next equation.

$$\bar{\phi}_B(X,p) = \frac{Nu\left[1-e^{-(p+Nu)X}\right]}{p^2(Bp+Nu+BNu)} + \frac{NuC_R \sin \pi KX}{p(p+Nu)(Bp+Nu)} - \frac{\pi KNuC_R\left[\cos \pi KX - e^{-(p+Nu)X}\right]}{p(p+Nu)^2(Bp+Nu)}. \quad (11)$$

Eq. (11) was inverted by use of the convolution theorem and a table of transforms, Roberts and Kaufmann [15]. It was then evident that $B = 1$ is a singular case and would have to be treated separately. Thus, the following result is for the general case, $B \neq 1$:

$$\phi_{Bqs}(X,F) = \left(\frac{Nu}{BW^2}\right)\left[e^{-WF} + WF - 1\right] + \left(\frac{C_R}{Nu}\right)\left[1 + \frac{\left(e^{-NuF} - Be^{-NuF/B}\right)}{B-1}\right] \times \sin \pi KX + A_2 \cos \pi KX, \quad (12)$$

$$W = Nu + \frac{Nu}{B}. \quad (13)$$

The coefficient A_2 depends upon B and F and is given in Appendix A.

Eq. (12) is now inserted into Eq. (8) and that differential equation is solved for $\phi_{Wqs}(X,F)$.

$$\phi_{Wqs}(X,F) = [b_6F - (b_0 + b_2 + b_3)]e^{-NuF/B} + b_0 + b_1F + b_2e^{-WF} + (b_3 + b_4F)e^{-NuF}, \quad (14)$$

$$b_4 = \frac{C_R \pi K \cos \pi KX}{Nu(1-B)^2}. \quad (15)$$

The other values b_0, b_1, etc. depend upon B and some also depend on $\sin \pi KX$. These values can be found in Appendix A. Eqs. (13) and (14) are for B not equal to 1.0. Only the calculated results for $B = 1.00$ will be shown in the figures.

For the generation rate given by Eq. (7), the overall procedure used parallels closely the one described above. Hence, the final results for ϕ_{Wqs} and ϕ_{Bqs} are given directly below for $B = 1.0$ for the generation $q'''/q_g = (e^{DF} - 1)\sin \pi KX$.

$$\phi_{Bqs}(X,F) = g_s \sin \pi KX + (g_{CA} + g_{CB}) \cos \pi KX. \quad (16)$$

Define,

$$J = Nu + D. \quad (17)$$

With this, the functions of time, g_s, g_{CA} and g_{CB}, can be written next.

$$g_s = \frac{Nu}{J^2}\left[e^{DF} - (1+JF)e^{-NuF}\right] - \frac{1}{Nu}\left[1 - (1+NuF)e^{-NuF}\right], \quad (18)$$

$$g_{CA} = \frac{\pi KNu}{J^3}\left[\left(1 + JF + .5J^2F^2\right)e^{-NuF} - e^{DF}\right], \quad (19)$$

$$g_{CB} = \frac{\pi K}{Nu^2}\left[1 - \left(1 + NuF + .5F^2Nu^2\right)e^{-NuF}\right]. \quad (20)$$

The quasi-steady solution for the wall temperature is given below.

$$\phi_{Wqs}(X,F) = C_s(F)\sin \pi KX + C_C(F)\cos \pi KX. \quad (21)$$

The time dependent coefficients in Eq. (21), $C_s(F)$ and $C_C(F)$, are given in Appendix A.

The constant flux Nu was used, $Nu = 2.055$, in all the quasi-steady calculations.

2.5. Analysis using approximate flux model

The development of the two integral flux model, for the first time domain, is presented in [12]. There it was found advantageous to use the following variable, τ, in place of the position variable X, $\tau = F - X$. Also used in the flux model was the following fully developed laminar velocity profile for the duct:

$$u(Y) = u_m\left[a_0Y + a_1Y^2\right], \quad a_0 = 3, \quad a_1 = -1.5. \quad (22)$$

With these, [12] gives the nondimensional heat flux, Q, shown next.

$$Q(F,\tau) = \frac{1}{\sqrt{\pi}}\left\{\int_0^F (F-\sigma)^{-1/2}\frac{\partial \phi_w}{\partial \sigma}d\sigma - \int_0^F \left[\frac{a_1\sqrt{F-\sigma}}{2\sqrt{\pi}} + \frac{a_0}{4} - \frac{(F-\sigma)^{-1/2}}{2\sqrt{\pi}}\right]\frac{\partial \phi_w}{\partial \tau}d\sigma\right\}. \quad (23)$$

Transforming Eq. (1), the energy balance on the wall, to the independent variables, F, τ, and inserting Eq. (23), yields the following integro-differential equation for $\phi_W(F,\tau)$:

$$\frac{\partial \phi_w}{\partial F} + \frac{\partial \phi_w}{\partial \tau} + \frac{1}{B\sqrt{\pi}}\int_0^F (F-\sigma)^{-1/2}\frac{\partial \phi_w}{\partial \sigma}d\sigma - \frac{1}{B\sqrt{\pi}}\int_0^F \left[\frac{a_1\sqrt{F-\sigma}}{2} + \frac{a_0\sqrt{\pi}}{4} - \frac{(F-\sigma)^{-1/2}}{2}\right] \times \frac{\partial \phi_w}{\partial \tau}d\sigma = \frac{f(F,\tau)}{B}. \quad (24)$$

In addition, the non-dimensional generation rates given in Eqs. (6) and (7) must have X replaced by $F-\tau$.

The fluid bulk mean temperature, $\phi_B(F,\tau)$, when the flux model, Eq. (23), is used is derived in [12] and shown below.

$$\phi_B(F,\tau)=\int_0^F\left[a_0+4a_1\frac{\sqrt{F-\sigma}}{\sqrt{\pi}}\right]\phi_W(\sigma,\tau)\,d\sigma+\int_0^F\left[-a_0(F-\sigma)+\left(\frac{8}{3}a_0^2-4a_1\right)\times\frac{(F-\sigma)^{3/2}}{\sqrt{\pi}}.+\frac{27}{4}a_0a_1(F-\sigma)^2+\frac{44a_1^2(F-\sigma)^{5/2}}{3\sqrt{\pi}}\right]\frac{\partial\phi_W}{\partial\tau}\,d\sigma. \quad (25)$$

Eq. (22) gives the values of a_0 and a_1 for the present problem. Once Eq. (24) is solved for ϕ_W, it can then be used in Eqs. (23) and (25) to give Q and ϕ_B.

In the present work, numerical procedures were used to solve Eqs. (24) and (25) for the generation rates given in Eqs. (6) and (7).

Using the superscript n to denote time, $F=n\Delta F$, and the index and subscript i to represent the X like variable $\tau=-i\Delta\tau$ where $\Delta\tau>0$, the following numerical representations were used for the partial derivatives in Eq. (24):

$$\frac{\partial\phi_W}{\partial F}\approx\frac{\phi_{W_i}^n-\phi_{W_i}^{n-1}}{\Delta F},\quad \frac{\partial\phi_W}{\partial\tau}\approx\frac{\phi_{W_i}^{n-1}-\phi_{W_{i+1}}^{n-1}}{\Delta\tau}. \quad (26)$$

The integrals appearing in Eq. (24) will be approximated by Riemann sums. The contribution to the first integral between $\sigma=(k-1)\Delta F$ and $\sigma=k\Delta F$ is shown next.

$$\int_{(k-1)\Delta F}^{k\Delta F}\frac{(F-\sigma)^{-1/2}}{\sqrt{\pi}}\frac{\partial\phi_W}{\partial\sigma}\,d\sigma\approx\frac{\left(\phi_{W_i}^k-\phi_{W_i}^{k-1}\right)}{\Delta F}R_k, \quad (27)$$

$$R_k=\frac{2}{\sqrt{\pi}}\left[\sqrt{F_a}-\sqrt{F_b}\right],\quad F_a=F-(k-1)\Delta F,\quad F_b=F-k\Delta F. \quad (28)$$

The same procedure was used for the second integral in Eq. (24), and leads to S_k.

$$S_k=\frac{a_1}{3\sqrt{\pi}}\left\{F_a^{3/2}-F_b^{3/2}\right\}+\frac{a_0\Delta F}{4}-\frac{R_k}{2}. \quad (29)$$

Next, inserting Eqs. (26), (28) and (29) into the energy balance, Eq. (24), and solving for $\phi_{W_i}^n$ gives the numerical representation for the solution for wall temperature.

$$\phi_{W_i}^n=\phi_{W_i}^{n-1}-\frac{\Delta F}{\Delta\tau}\left(\phi_{W_i}^{n-1}-\phi_{W_{i+1}}^{n-1}\right)M\left(1-\frac{S_n}{B}\right)-M\sum_{k=1}^{n-1}\frac{R_k}{B}\left(\phi_{W_i}^k-\phi_{W_i}^{k-1}\right)+\frac{M}{B}\frac{\Delta F}{\Delta\tau}\sum_{k=1}^{n-1}S_k\left(\phi_{W_i}^{k-1}-\phi_{W_{i+1}}^{k-1}\right)+\frac{M}{B}\Delta Ff(F,\tau),$$
$$M=B/(B+R_n) \quad (30)$$

The bulk mean fluid temperature, given in Eq. (25), when using the approximate flux model, Eq. (23), can be evaluated numerically once $\phi_W(F,\tau)$ is known. The numerical representation of Eq. (25) follows that of Eq. (24).

Similarly, the evaluation of the surface heat flux, Q, is given next.

$$Q=\sum_{k=1}^{n}R_k\left(\frac{\phi_{W_i}^k-\phi_{W_i}^{k-1}}{\Delta F}\right)-\sum_{k=1}^{n}S_k\left(\frac{\phi_{W_i}^{k-1}-\phi_{W_{i+1}}^{k-1}}{\Delta\tau}\right). \quad (31)$$

The needed values of the index i, which through τ fixes the space location, X, are determined from the relation between F, X and τ, namely, $X=F+i\Delta\tau$.

A computer program was written to solve Eq. (30) for ϕ_W which was then used to find ϕ_B and Q as functions of space, X, and time, F, for the wall generation rates given by Eqs. (6) and (7). A rough stability analysis of Eq. (30) indicates conditional stability as long as $\Delta F\leqslant\Delta\tau$, at least for $B\geqslant 0.10$. In fact, experience gained in using the program indicates that when possible, ΔF should be chosen to be equal to $\Delta\tau$. Lattice size studies indicated that when $f(X,F)$ is given by Eq. (7) with $D=4.0$, $K=1.0$ and $B=1.0$, lattice sizes $\Delta F=\Delta\tau=0.0005$ were needed for $F\geqslant 0.05$. Spacings of ΔF and $\Delta\tau$ of one half this value cause, at most, a 0.70% change in ϕ_B, a 0.45% change in ϕ_W and a 0.30% change in Q.

3. Results and discussion

The first six figures are all for the generation rate per unit volume, q''', given by $q'''/q_g=1+C_R\sin\pi KX$. All of the figures show the baseline finite difference solution to illustrate the general trends of ϕ_W with time, F, position X and thermal capacity ratio of the wall material to the fluid, B. The figures also contain a more limited representation of these trends for ϕ_B and Q. Comparisons between the baseline finite difference solution and both the quasi-steady results and the results using the two integral approximate flux model are made in some of the figures. Some figures show results only in time domain I, where $F\leqslant(2/3)X$, since both quasi-steady and the approximate flux model are, strictly speaking, limited to this first time domain.

However, some base line finite difference results are given also in time domain II since this solution is not limited to just the first time domain. Some comparisons are made to results predicted by the quasi-steady and approximate flux model for time $F > (2/3)X$ to see how they perform.

Fig. 1 shows the finite difference solution for ϕ_W versus time, F, at various values of B as the solid curves, while the dashed curves are the corresponding quasi-steady results. These are plotted at the position $X = 0.50$, using $C_R = 1$ and $K = 1$ in the generation rate, with time domain I results for $F \leqslant 0.333$. It is seen that the quasi-steady results can be greatly in error, as is evident for $B = 0.1$, 0.5 and 1.0, but, as B increases, they are approaching the finite difference result, particularly for $B = 10.0$. At $B = 10.0$, the quasi-steady predictions of ϕ_W are only in error by about 1.5% while at $B = 2.0$, the error has already increased to 6.5%. The results predicted by the approximate flux model are not shown explicitly in this figure because they are so close to the baseline finite difference results (maximum difference less than 0.9%) that they cannot be distinguished from them in the curve plots.

Fig. 2 is for the same set of conditions as Fig. 1, but plots the fluid bulk mean temperature, ϕ_B, versus time F. Once again the quasi-steady results, the dashed curves,

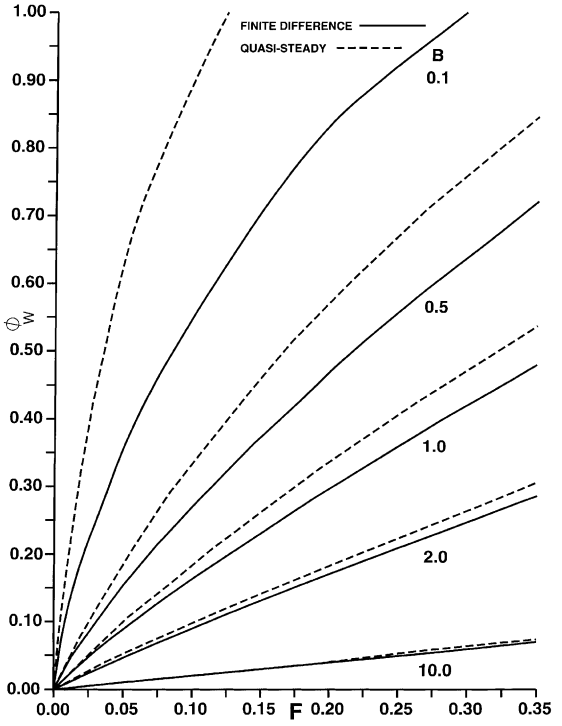

Fig. 1. Prediction of wall temperature, ϕ_w, versus time, F, at position $X = 0.50$ showing influence of B. Sinusoidal in X wall generation.

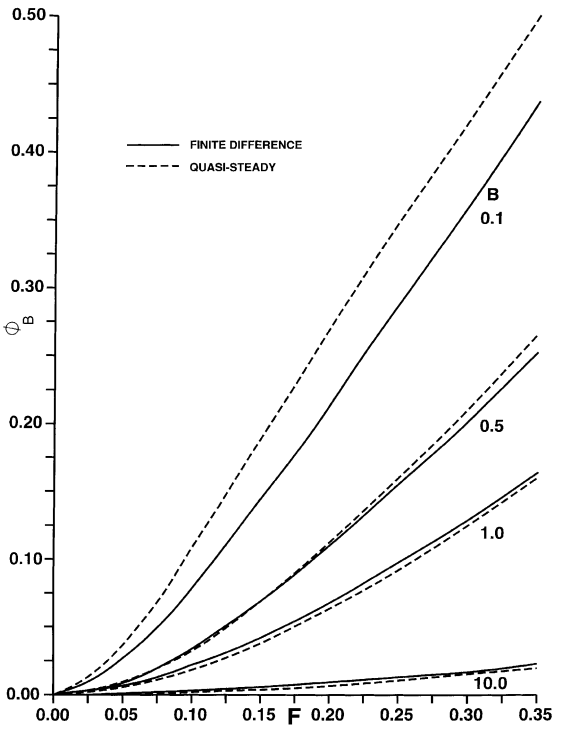

Fig. 2. Predicted fluid temperature, ϕ_B, at $X = .50$, versus time, F, showing influence of B. Wall generation sinusoidal in X.

tend to approach the baseline finite difference predictions as B increases. However, unlike ϕ_W, the error in the quasi-steady value of ϕ_B is still significant at $B = 10.0$. It ranges from about 23% at $F = 0.05$ to 10% at $F = 0.35$. The size of this difference is not apparent from the curves at $B = 10.0$ because of the small values of ϕ_B at this condition. In fact, the error, percentage-wise, is smaller at $B = 0.5$ than it is at $B = 10.0$. Another general trend, which is not obvious from a direct look at the figure, is that, for all values of B, the quasi-steady results get closer to the finite difference results as time, F, increases. In general, as is known, the slower the transient, the better the quasi-steady predictions since slow transients are connected with low surface fluxes, Q. Low surface heat flux is a hallmark of quasi-steady analysis because of the use of the fully developed, steady state, value of the surface coefficient, h, which is always lower than the true unsteady value. Again, as is also true in Fig. 1, the results of the two integral flux model are virtually indistinguishable from the baseline results, a maximum difference of about 1.1%, so they were not plotted separately.

Fig. 3 gives the finite difference results for ϕ_W as a function of position X and its evolution in time, F, for $B = 0.1$ and 1.0. These results are not limited to the first time domain. In this figure, the results for time domain I are shown as solid curves while the dashed portion of

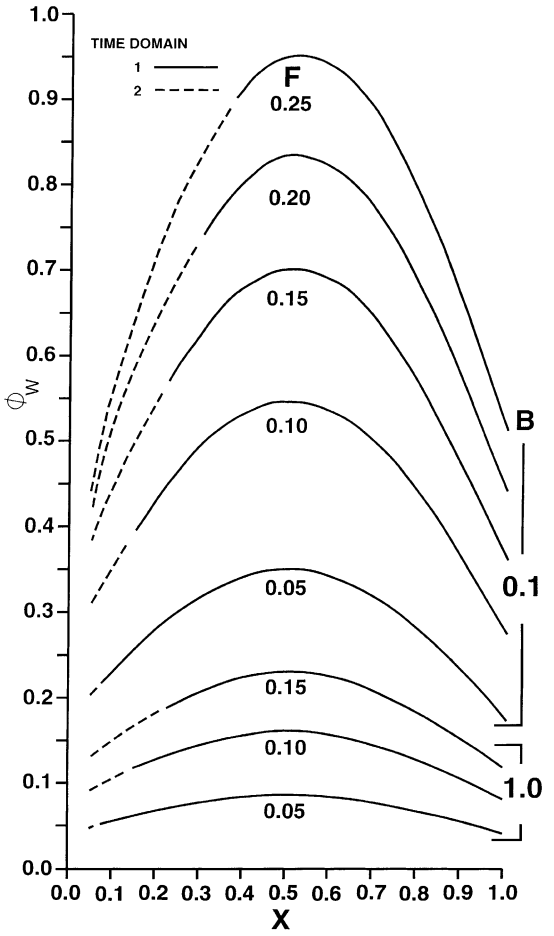

Fig. 3. Wall temperature, ϕ_w, variation with position, X, and time F. Wall generation sinusoidal in X.

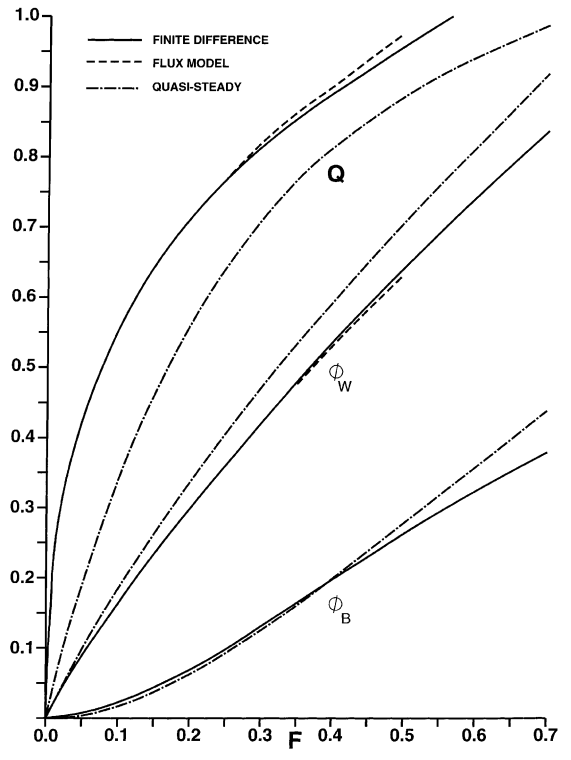

Fig. 4. Prediction of Q, ϕ_w and ϕ_B by three different models at $X = .50$ and for $B = 1.00$. Wall generation sinusoidal in X.

each curve shows ϕ_W in the second time domain, $F > (2/3)X$. The overall trend of ϕ_W with X is about what is expected, considering that the generation rate is sinusoidal with X.

The baseline solution, solid curves, the quasi-steady solution, large dash-small dash and the approximate flux model, the dashed curves, are compared in Fig. 4 at $X = 0.5$ for $B = 1.0$. These comparisons are made beyond the end of the first time domain, $F \leqslant 0.333$ for $X = .5$, to include a portion of the second domain, $F > 0.333$. The quasi-steady and the flux model solutions are first time domain solutions which are forced to make calculations into the second domain as a test to see how long they will give reasonable accuracy. In the first time domain, $F \leqslant 0.333$, the quasi-steady predictions parallel the behavior seen earlier in Figs. 1 and 2, namely, its ϕ_W is too high by about 12% and its ϕ_B is too low by 16% at $F = .05$ to about 2% at $F = 0.333$. The reason for this is evident by looking at the flux, Q, in Fig. 4. It is low for the quasi-steady, due to the use of too low a surface coefficient, leading to more of the wall generation staying in the wall giving a higher than correct ϕ_W and less going to the fluid causing a lower ϕ_B than that given by the baseline solution. On the other hand, the approximate flux model, the dashed curve, is practically coincident with the ϕ_W and ϕ_B finite difference curves up to $F = 0.333$ with a maximum error of 0.45% for ϕ_W and 1% for ϕ_B at $F = 0.05$ where ϕ_B is very low. Inherent limitations in the approximate flux model restrict its ability to calculate outside of the first time domain to $F = 0.5$ at $X = .5$. However, in this region, $0.333 < F < 0.5$, the model still does very well with maximum error in ϕ_W and ϕ_B being 1.5% and 0.75%, respectively, at $F = 0.50$. It should also be pointed out that the approximate model, theoretically restricted to the thermal entrance length, is calculated beyond the thermal entrance region which occurs at about $F = 0.15$, for $X = .50$, as determined by the finite difference solution. Probably this is a factor in the error of the approximate model.

In Fig. 5, the limitations of the approximate flux expression, Eq. (23), were explored further. Shown are plots of ϕ_W, ϕ_B and Q versus time, F, at $X = 1.0$ and $B = 2.0$, for the baseline solution and for the approximate flux model. At $X = 1.0$, the end of the first time

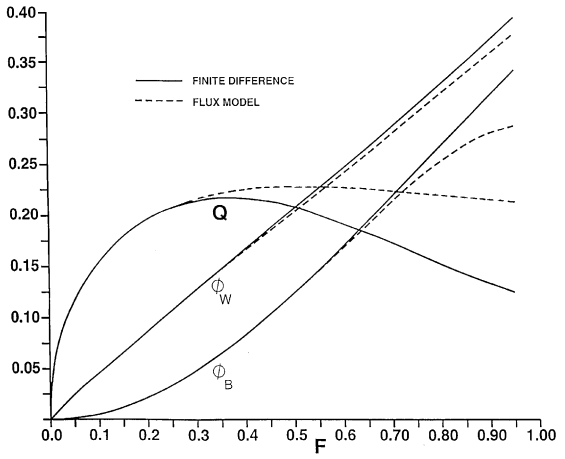

Fig. 5. Approximate flux model predictions compared to finite difference results at $X = 1.0$ and for $B = 2.00$. Wall generation sinusoidal in X.

domain is at $F = 0.666$. The model solution, dashed curves, predicts ϕ_W and ϕ_B fairly well up to $F = .666$ in spite of the fact that the Q prediction has a significant error beyond $F = 0.4$. The error in the model is 1.8% and 1.4% for ϕ_W and ϕ_B at $F = .666$. This error increases to 4% for ϕ_W and 16% for ϕ_B at $F = 0.95$. The reasons for this are that the flux model is being used beyond the end of the time domain for which it was derived, that is, beyond $F = .666$ at $X = 1.0$ and is also being used well beyond the end of the thermal entrance region, which is at about $F = 0.15$ for this case. Taking Figs. 4 and 5 together, it is seen that the approximate model predictions will degenerate as the location, X, at which the calculations are made, increases.

ϕ_W for both the finite difference and the quasi-steady solutions is plotted in Fig. 6 versus X at time $F = .20$ for a wide range of B to investigate the quasi-steady solution's accuracy at various positions along the wall. The finite difference results are represented by the solid curves and the quasi-steady by the long dash-short dashed curves in the first time domain. Both solutions are given by the dashed portion of each curve in the second time domain, $F > (2/3)X$ for the finite difference and $F > X$ for the quasi-steady. Evident again is the increasing error in quasi-steady predictions as B gets smaller. The average error increases from about 1.5% at $B = 10.0$, where the quasi-steady solution is not plotted since it falls virtually on top of the finite difference results for plotting purposes, to an error of about 30% at $B = 0.3$. The error in the quasi-steady results decreases slowly with increasing X values, but does not vary very much with X. At $B = 0.3$ this error varies from 38% at $X = 0.05$ to 28% at $X = 1.0$ while at $B = 10.0$, it varies from 1.8% at $X = 0.05$ to 1.4% at $X = 1.0$. Very roughly, it was found that this error was approximately

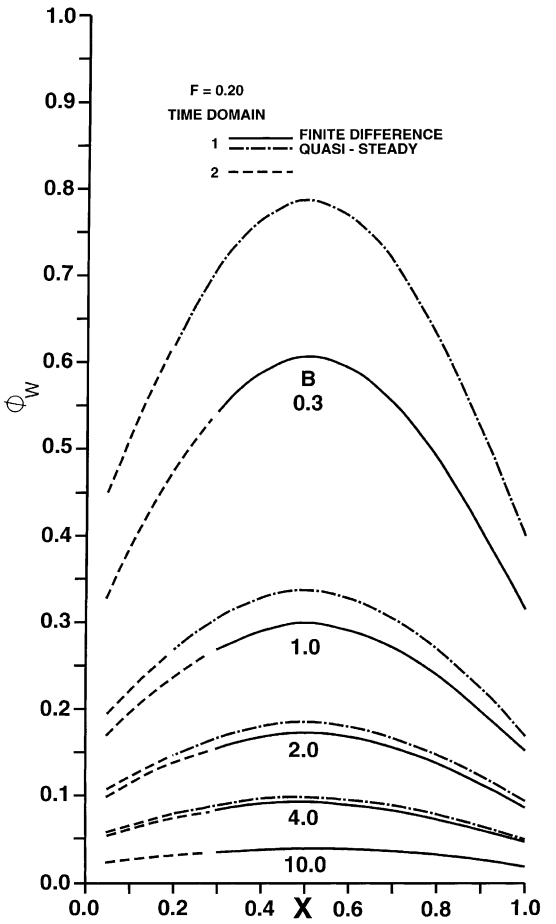

Fig. 6. Quasi-steady wall temperature predictions compared to finite difference results at time, $F = 0.20$ for a range of values of B. Wall generation sinusoidal in X.

doubled for every halving of the value of B. Once again it is noted that the quasi-steady results for the wall temperature are very close to the baseline results when B becomes as large as 10.0. This has been noted previously for a different kind of transient in [16]. The choice of the range of B values used in the present work was determined by the work in [16–18]. As with some previous figures, the results for the approximate flux model were not plotted in Fig. 6 because they essentially lie on top of the finite difference curves. The maximum difference between them is about 0.5%. It will be recalled that the dashed portions of the curves in Fig. 6 are the portions in time domain II. At time $F = .20$ for $X < 0.20$, calculations are still being made in the first time domain for the quasi-steady and approximate flux model. Apparently, this is not far enough into the second time domain yet, because these results, when compared to the baseline finite difference solution, have about the same accuracy as they had in the first time domain.

The last three figures are all for the generation rate per unit volume given by Eq. (7), where q''' depends upon both position X and time F, namely, $q'''/q_g = (e^{DF} - 1)\sin \pi KX$.

Fig. 7 displays the finite difference results (solid curves) and the quasi-steady predictions (long dash-short dash) for ϕ_W, ϕ_B and Q as a function of F at $X = 0.50$ and ϕ_W for $X = 0.20$. The parameters D and K are chosen equal to 4.0 and 1.0, respectively while $B = 1.0$. The rapid increase of these quantities with F, due to the exponential growth factor, e^{4F}, in the generation, is evident. The error in the quasi-steady ϕ_W averages about 12–14%, while that for ϕ_B ranges from 19% at $F = 0.05$ down to 0.4% at $F = 0.50$. The quasi-steady solution underpredicts Q and ϕ_B and overpredicts ϕ_W for the reasons mentioned earlier with the other generation rate. Results using the approximate flux model, again, lie virtually on top of the finite difference predictions with a maximum deviation of about 0.6%.

The duct wall temperature variation with X, at various times, F, during the transient is shown in Fig. 8. The

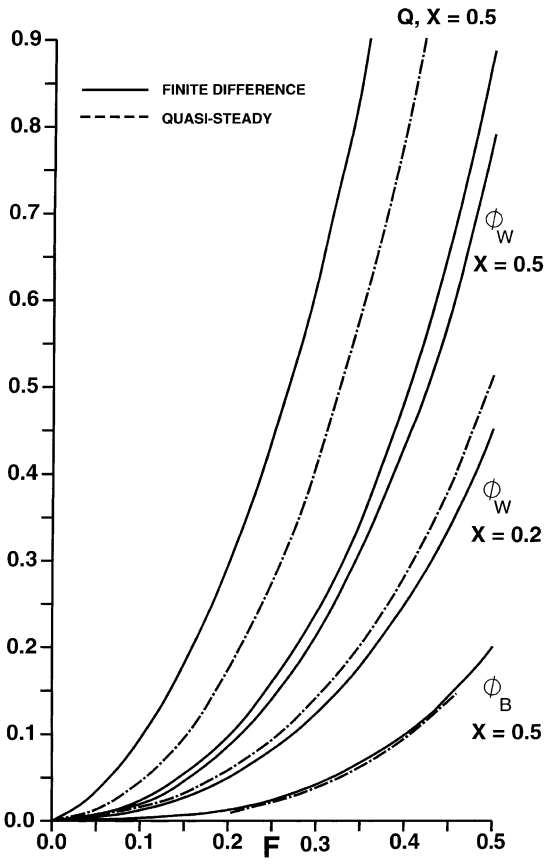

Fig. 7. Predictions of ϕ_w, ϕ_B and flux, Q, at $X = .50$ for $B = 1.0$ for wall generation exponential in time, F, and sinusoidal in X. $D = 4.0$.

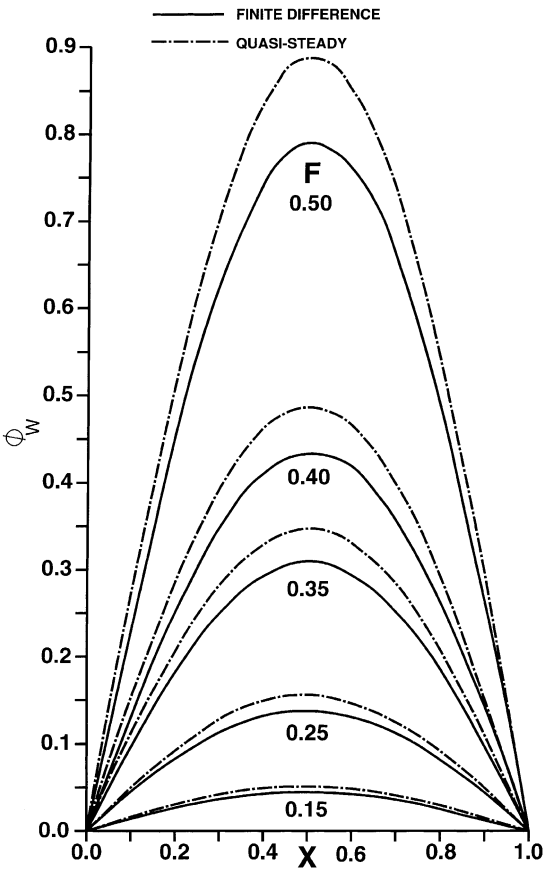

Fig. 8. Evolution of wall temperature, ϕ_w, with time, F, and position X for $B = 1.0$ and $D = 4.0$. Wall generation exponential in F and sinusoidal in X.

quasi-steady results exhibit an error which increases as F increases from 0.15 to 0.50. This is due to the fact that the quasi-steady solution satisfies the initial condition, that at $F = 0$, $\phi_W = 0$, and therefore begins with no error at all. The error is seen to progressively increase from this as the time F gets farther away from $F = 0$. The average error, from $F = .05$ to $F = .50$, in the quasi-steady prediction of ϕ_W is about 15% at $X = .10$ gradually decreasing to about 10% at $X = .90$ while for ϕ_B the average error is about 30% at $X = .10$ and about 7% at $X = .90$. Some of this error may be due to the use of the first time domain quasi-steady relations to perform calculations in the second time domain. For instance, at $X = .10$, all values of $F > .10$ are in the second time domain for the quasi-steady analysis. At $X = 1.00$, the wall temperature predictions for the quasi-steady are greatly in error. It is felt that this is probably due to the generation, q''', being zero at $X = 1.0$, therefore, the wall temperature rise is due solely to convection from the fluid to the wall. Hence, the small value of the heat transfer coefficient, h, causes the quasi-steady solution to

underpredict the temperature there while at upstream locations the positive generation causes convection to the fluid and the small value of h gives an overprediction of ϕ_W. Because of the very small values of ϕ_W very close to $X = 1.0$, this underprediction of ϕ_W cannot be detected in Fig. 8.

In a conjugated heat transfer problem, since neither the surface heat flux, Q, nor the wall temperature, ϕ_W, is known, either the heat transfer coefficient, h, or, equivalently, the Nusselt number, $Nu = hR/k_f$, is not of as much interest and value as in a non-conjugated problem. Actually, even in a non-conjugated problem, the surface temperature variation with X may be such that the Nusselt number and the heat transfer coefficient cease to have much value and significance, as pointed out in [19]. However, engineers working in industry are used to using the Nusselt number in convection heat transfer calculations, so it seemed worthwhile to present some transient Nusselt number predictions. This is shown in Fig. 9, where the transient Nusselt number at $X = 0.5$ is graphed as a function of time for different values of the thermal capacity ratio, B, and for a number of values of the coefficient, D, in the exponent of the generation rate given by Eq. (7).

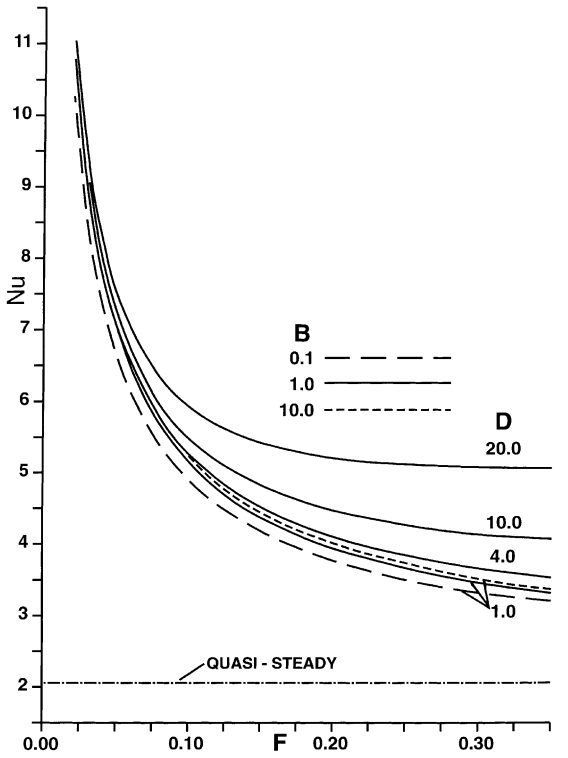

Fig. 9. Predicted transient Nusselt number, Nu, with time, F, at $X = 0.50$ showing trends with B and D variation, wall generation exponential in time, F, and sinusoidal in X.

There are a number of interesting features illustrated by Fig. 9. Of notice first are the high values of the Nusselt numbers predicted by the baseline finite difference solution (the six highest curves) when compared to the value used to get the quasi-steady solution, 2.055, shown as the horizontal line near the bottom of the figure. This is a characteristic of a quasi-steady analysis, as mentioned previously. All Nusselt number curves begin at infinity at $F = 0$ and rapidly decrease with time before a period in which they slowly decrease with time, F. This is caused by the zero thickness of the thermal boundary layer at $F = 0$ followed by its growth toward $y = R$ at the end of the thermal entrance region. The lowest three curves in Fig. 9 show the dependence of the Nusselt number on the storage ratio, B, when $D = 1.0$, with Nu increasing as B increases from 0.1 to 10.0. The maximum difference between Nu at $B = .1$ and Nu at $B = 10.0$ is less than 7%, hence, the value of B does not exert much influence on the Nusselt number for this generation rate. On the other hand, Fig. 9 shows a stronger dependence of the Nusselt number on the coefficient, D, in the exponential with time, F, generation, $q''' = q_g(e^{DF} - 1)\sin \pi KX$. At $F = 0.35$, Nu when $D = 20$ is 52% higher than its value at $D = 1$. This is illustrated by the four curves for $B = 1.00$ for values of D equal to 1, 4, 10 and 20.

As mentioned earlier, all of the transient values of Nu in Fig. 9 are higher than the value, $Nu = 2.055$, used by the quasi-steady analysis. However, as has been pointed out in [7], a comparison of the Nusselt numbers is not the proper way to measure the performance of a quasi-steady analysis, rather the proper assessment of its accuracy should be made by comparing the predicted wall temperature, ϕ_W, and the fluid bulk mean temperature, ϕ_B, with baseline results for these two temperatures, as has been done in the previous figures.

The Nu predictions of the approximate, two integral heat flux model, Eq. (23), as in previous figures, lie on top (as far as plotting ability is concerned) of the finite difference results in Fig. 9 for $B = 1.0$ and $D = 4.0$. The maximum difference between them is around 0.1%. Initially, it was hoped that the approximate flux model would not only allow an analytical solution to simple enough transient conjugate problems as it did in the earlier work [14], but that it would also be a better choice than finite difference solutions of the partial differential equation in problems that were done numerically as with Eq. (30). However, in the present work, it was found that solving the flux model equations numerically, Eqs. (23)–(25), often took more computer time than that needed to solve the finite difference equations, Eq. (5) of the present paper along with Eqs. (8) and (9) of reference [7]. In retrospect, it is felt that this is due to the inherent nature of the "historic" integrals of Eq. (23), the flux model. As can be seen by looking at the numerical representation of this equation,

namely, Eq. (31), a calculation made at time, $\imath = n\Delta\imath$ requires the use of ϕ_w^k, R_k and S_k at every value k less than n, that is $k = 1, 2, 3, \ldots, n-1$. Thus, the computer must store and then recall the entire previous time "history" of these quantities to make the calculations at the present time, $n\Delta t$. The finite difference solution, on the other hand, only requires storage of ϕ_W at the previous time, $(n-1)\Delta t$, to calculate ϕ_W at the present time, $n\Delta t$. In an attempt to reduce the computer computation time for the flux model in numerical form, Eq. (31), it was thought that perhaps the summation index k could be started at values greater than 1, like $k = k_s$ where k_s is reasonably close to $n-1$ in the summations required in Eqs. (30) and (31). The basis for trying this was the thought that maybe the most recent previous history in time was the most important as far as contributions to the summation's values are concerned. But numerical experiments trying this indicated a significant loss of accuracy in the results for any worthwhile decrease in computer run time.

So, even though the two integral flux model for the first time domain, Eq. (23), is very accurate, giving results that are virtually identical with the baseline finite difference solution, a numerical solution employing it, such as Eq. (30), cannot, in general, be recommended over a direct finite difference solution of the partial differential equation. However, it is recommended for problems in which an analytical solution is feasible and it has been successfully used to arrive at an analytical solution as was demonstrated in [14].

4. Conclusion

Three different approaches are presented for the solution of the class of transient, conjugated duct flow problems when there is time and space dependent generation within the duct wall material. These methods are first, an implicit finite difference solution of the governing partial differential equations giving the baseline solution, second, a quasi-steady solution and, last, a solution which uses a two integral, approximate expression for the surface heat flux. The last two methods above are, in theory, limited to the first time domain while the finite difference solution has no such limitation.

Baseline predictions have been made for wall temperature, fluid bulk mean temperature and wall heat flux as functions of both position and time. Results from the other two methods are compared to these finite difference results.

Once again, as has also been the case for earlier work in the literature involving different types of transients, it is concluded that if $B \geqslant 10$, the quasi-steady wall temperature predictions may be judged to be of adequate accuracy. However, this might not be true for the fluid bulk mean temperature prediction.

The two integral expression for the surface heat flux, though it is an approximate model, has been shown to be highly accurate with results practically identical to those of the baseline finite difference solution in the first time domain. Therefore, it is highly recommended for use when there exists the possibility of an analytical solution to an unsteady conjugate problem. However, in general, it cannot be recommended for use when numerical methods are required for its evaluation, except at very small times. This is not a question of its accuracy, but rather, it is due to longer computer run times than the direct finite difference baseline solution.

Calculations indicate the possibility of using the flux model beyond the end of the first time domain for a short time into the second time domain and retaining high accuracy. This is especially true at lower values of position, X. The quasi-steady solution can also be used for a time beyond the first time domain with accuracy comparable to what it had in the first time domain.

The predicted transient Nusselt number was found to be only weakly dependent upon the thermal capacity ratio, B, but strongly dependent upon the rapidity of the transient as measured by the coefficient of time in the exponential, with time, generation rate.

Appendix A

$$A_2 = -\frac{C_R \Pi K B}{Nu^2 (B-1)^2}\left[\frac{(2B-1)}{B}e^{-NuF} + \frac{(B-1)}{B}NuF e^{-NuF} + \frac{(B-1)^2}{B} - B e^{-\frac{NuF}{B}}\right]. \quad (A.1)$$

Coefficients in Eqs. (14) and (21).

$$b_0 = \frac{B}{Nu}\left[\frac{1}{B} + 2G_S - G_0 + G_C\left(B - \frac{1}{B} - 2\right) - \frac{BG_0W}{Nu}\right],$$

$$G_S = \frac{C_R}{B}\sin \Pi K X, \quad G_0 = \left(\frac{Nu}{BW}\right)^2, \quad (A.2)$$

$G_C = -b_4$ (given in Eq.(15)),

$$b_1 = \frac{BG_0W}{Nu},\ b_2 = \frac{BG_0}{Nu - BW},\ b_3 = \frac{\frac{G_S}{B-1} + G_C\left(3 - \frac{1}{B}\right)}{\frac{Nu}{B} - Nu},$$

$$b_6 = -B\left[\frac{G_S}{(B-1)} + G_C\right], \quad (A.3)$$

$$C_S = -\frac{Nu g_{CA}}{\Pi K} + \frac{1}{J}\left(e^{DF} - e^{-NuF}\right) + C_{SB}, \quad (A.4)$$

$$C_{SB} = \frac{1}{Nu}\left[\left(2 + NuF + Nu^2F^2\right)e^{-NuF} - 2\right], \quad (A.5)$$

g_{CA} is given by Eq. (19) in the main body of the text.

$$C_c = \frac{Nu}{J}g_{CA} + g_{CB} + \left(\frac{Nu}{J} - 1\right)\frac{\Pi K Nu F^3 e^{-NuF}}{6}, \quad (A.6)$$

g_{CA} and g_{CB} are given by Eqs. (19) and (20) in the main body of the paper.

References

[1] D.J. Schutte, M.M. Kahman, A. Faghri, Transient conjugate heat transfer in a thick walled pipe with developing laminar flow, Numer. Heat Transfer, Part A 21 (1992) 163–186.

[2] M.A. Al-Nimr, M.A. Hader, Transient conjugated heat transfer in developing laminar pipe flow, ASME J. Heat Transfer 116 (1994) 234–236.

[3] W.M. Yan, Y.L. Tsay, T.F. Lin, Transient conjugated heat transfer in laminar pipe flows, Int. J. Heat Mass Transfer 32 (4) (1989) 775–777.

[4] T.F. Lin, J.C. Kuo, Transient conjugated heat transfer in fully developed laminar pipe flows, Int. J. Heat Mass Transfer 31 (1988) 1093–1102.

[5] S. Olek, Unsteady conjugated heat transfer in laminar pipe flow, Int. J. Heat Mass Transfer 34 (1991) 1443–1450.

[6] W.M. Yan, Transient conjugated heat transfer in channel flows with convection from the ambient, Int. J. Heat Mass Transfer 36 (5) (1993) 1295–1301.

[7] J. Sucec, Unsteady conjugated forced convection heat transfer in a duct with convection from the ambient, Int. J. Heat Mass Transfer 30 (1987) 1963–1970.

[8] J.S. Travelho, W.F.N. Santos, Unsteady conjugate heat transfer in a circular duct with convection from the ambient and periodically varying inlet temperature, ASME J. Heat Transfer 120 (1998) 506–510.

[9] R.O.C. Guedes, M.N. Ozisik, R.M. Cotta, Conjugated periodic turbulent forced convection in a parallel plate channel, ASME J. Heat Transfer 116 (1994) 40–46.

[10] R. Siegel, Forced convection in a channel with wall heat capacity and with wall heating variable with axial position and time, Int. J. Heat Mass Transfer 6 (1963) 607–620.

[11] F.E. Romie, Response of counterflow heat exchangers to step changes of flow rates, ASME J. Heat Transfer 121 (3) (1999) 746–748.

[12] J. Sucec, D. Radley, Unsteady forced convection heat transfer in a channel, Int. J. Heat Mass Transfer 33 (1990) 683–690.

[13] D.A.S. Rees, The effect of steady streamwise surface temperature variations on vertical free convection, Int. J. Heat Mass Transfer 42 (1999) 2455–2464.

[14] J. Sucec, H. Weng, Transient conjugate convective heat transfer in a duct with wall generation, in: M.K. Jensen, M. DiMarzo (Eds.), Proceedings of the 33rd National Heat Transfer Conference, ASME, Albuquerque, NM, 1999, NHTC99-61.

[15] G.E. Roberts, H. Kaufmann, Tables of Laplace Transforms, W.B. Saunder, Philadelphia, PA, 1966.

[16] J. Sucec, Exact solution for unsteady conjugated heat transfer in the thermal entrance region of a duct, ASME J. Heat Transfer 109 (1987) 295–299.

[17] F.E. Romie, Transient response of crossflow heat exchangers with zero core thermal capacitance, ASME J. Heat Transfer 116 (1994) 775–777.

[18] R. Karvinen, Transient conjugated heat transfer to laminar flow in a tube or channel, Int. J. Heat Mass Transfer 31 (1988) 1326–1328.

[19] W.M. Kays, M.E. Crawford, in: Convective Heat Mass Transfer, third ed., McGraw-Hill, New York, 1993, pp. 144–146.